Universiteit Leiden
The Netherlands

Automatic three-dimensional magnetic resonance-based measurements of tumour prominence and basal diameter for treatment planning of uveal melanoma

Klaassen, L.; Jaarsma-Coes, M.G.; Verbist, B.M.; Vu, T.H.K.; Marinkovic, M.; Rasch, C.R.N.; ... ; Beenakker, J.W.M.

Citation
Klaassen, L., Jaarsma-Coes, M. G., Verbist, B. M., Vu, T. H. K., Marinkovic, M., Rasch, C. R. N., … Beenakker, J. W. M. (2022). Automatic three-dimensional magnetic resonance-based measurements of tumour prominence and basal diameter for treatment planning of uveal melanoma. *Physics & Imaging In Radiation Oncology*, *24*, 102-110. doi:10.1016/j.phro.2022.11.001

Version: Publisher's Version
License: Creative Commons CC BY-NC-ND 4.0 license
Downloaded from: https://hdl.handle.net/1887/3566454

Note: To cite this publication please use the final published version (if applicable).

Physics and Imaging in Radiation Oncology 24 (2022) 102–110

Contents lists available at ScienceDirect

Physics and Imaging in Radiation Oncology

journal homepage: www.sciencedirect.com/journal/physics-and-imaging-in-radiation-oncology

Original Research Article

Automatic Three-Dimensional Magnetic Resonance-based measurements of tumour prominence and basal diameter for treatment planning of uveal melanoma

Lisa Klaassen [a,b,c,*], Myriam G. Jaarsma-Coes [a,b], Berit M. Verbist [b,d], T.H. Khanh Vu [a], Marina Marinkovic [a], Coen R.N. Rasch [c,d], Gregorius P.M. Luyten [a], Jan-Willem M. Beenakker [a,b,c]

[a] Leiden University Medical Center, Department of Ophthalmology, PO Box 9600, 2300 RC Leiden, the Netherlands
[b] Leiden University Medical Center, Department of Radiology, PO Box 9600, 2300 RC Leiden, the Netherlands
[c] Leiden University Medical Center, Department of Radiation Oncology, PO Box 9600, 2300 RC Leiden, the Netherlands
[d] Holland Particle Therapy Center, PO Box 110, 2600 AC Delft, the Netherlands

ARTICLE INFO

Keywords:
Uveal melanoma
Ocular oncology
Magnetic resonance imaging
Ultrasound

ABSTRACT

Background and Purpose: Three-dimensional (3D) Magnetic Resonance Imaging (MRI) is increasingly used to complement conventional two-dimensional ultrasound in the assessment of tumour dimension measurement of uveal melanoma. However, the lack of definitions of the 3D measurements of these tumour dimensions hinders further adaptation of MRI in ocular radiotherapy planning. In this study, we composed 3D MR-based definitions of tumour prominence and basal diameter and compared them to conventional ultrasound.
Materials and methods: Tumours were delineated on 3DT2 and contrast-enhanced 3DT1 (T1gd) MRI for 25 patients. 3D definitions of tumour prominence and diameter were composed and evaluated automatically on the T1gd and T2 contours. Automatic T1gd measurements were compared to manual MRI measurements, to automatic T2 measurements and to manual ultrasound measurements.
Results: Prominence measurements were similar for all modalities (median absolute difference 0.3 mm). Automatic T1gd diameter measurements were generally larger than manual MRI, automatic T2 and manual ultrasound measurements (median absolute differences of 0.5, 1.6 and 1.1 mm respectively), mainly due to difficulty defining the axis of the largest diameter. Largest differences between ultrasound and MRI for both prominence and diameter were found in anteriorly located tumours (up to 1.6 and 4.5 mm respectively), for which the tumour extent could not entirely be visualized with ultrasound.
Conclusions: The proposed 3D definitions for tumour prominence and diameter agreed well with ultrasound measurements for tumours for which the extent was visible on ultrasound. 3D MRI measurements generally provided larger diameter measurements than ultrasound. In anteriorly located tumours, the MRI measurements were considered more accurate than conventional ultrasound.

1. Introduction

Uveal melanoma (UM) is the most frequently occurring primary intraocular malignancy [1]. For UM, tumour location and dimensions are major factors in treatment decision making, as only tumours up to a certain size can be treated with brachytherapy [1–3], whereas larger and juxtapapillary UM are preferably treated with external beam radiotherapy, such as proton beam therapy (PBT) or Cyber Knife [4–6]. Furthermore, tumour prominence and diameter measurements are of importance for radiotherapy planning: in brachytherapy, prominence and largest basal diameter (LBD) determine the application time and applicator size, while for PBT, these two-dimensional (2D) tumour measurements, together with the second basal diameter (SBD) are important factors in the definition of three-dimensional (3D) clinical target volume [2,7]. Additionally, prominence, LBD and SBD are used in tumour staging, prognosis and follow-up [8–12].

* Corresponding author at: Postal Zone J3-S, PO Box 9600, 2300 RC Leiden, the Netherlands.
E-mail address: l.klaassen@lumc.nl (L. Klaassen).

https://doi.org/10.1016/j.phro.2022.11.001
Received 15 August 2022; Received in revised form 31 October 2022; Accepted 1 November 2022
Available online 6 November 2022
2405-6316/© 2022 The Authors. Published by Elsevier B.V. on behalf of European Society of Radiotherapy & Oncology. This is an open access article under the CC BY-NC-ND license (http://creativecommons.org/licenses/by-nc-nd/4.0/).

Conventionally, tumour prominence and diameters are determined using 2D B-scan ultrasound [1]. For a correct prominence measurement, the transducer has to be positioned perpendicular to the tumour base, as oblique cuts through the tumour can result in overestimation of the true tumour prominence [13]. For anterior tumours, correct transducer placement might be hindered due to anatomical structures around the eye [14]. Additionally, to correctly determine the LBD, the longest tumour axis has to be identified, which can be difficult as no 3D visualization is available.

Magnetic resonance imaging (MRI) is increasingly used for the diagnosis, therapy planning and follow-up of UM [7,15–20]. Various studies suggest that MRI's 3D tumour visualisation and better tissue contrast might be beneficial in determining UM tumour dimensions compared to conventional 2D ultrasound, corresponding to findings in other malignancies [16–24]. Nevertheless, several uncertainties in MR-based dimensions measurements for ocular tumours remain that hinder broader application of MRI in ocular radiotherapy planning, for example regarding the optimal method to measure in 3D and the differences related to the various MRI contrasts.

Although the 3D visualisation of the tumour of MRI allows for a more comprehensive assessment of tumour geometry [18], tumour dimension measurements can be performed in different planes, resulting in different possible prominence and diameter measurements, especially for complexly shaped tumours (Fig. 1) [19,25]. Additionally, manual measurement of prominence and LBD on MRI is reported to be difficult and time-consuming [26]. Therefore, the current clinical practice might benefit from automated tumour prominence and diameter measurements, using an unambiguous geometrical definition. Furthermore, studies showed an 11–44 % larger tumour volume on contrast-enhanced T1-weighted images (T1gd) compared to T2-weighted images [21,27]. Although such a difference between MRI sequences is not uncommon [28,29], these differences should be kept in mind when defining optimal measurements.

In this study, we aimed to compose and evaluate a geometrical 3D definition of prominence and diameters.

2. Materials and methods

Data of 25 patients, who received an MRI as part of clinical care (n = 17) or in the context of a scientific study (n = 8), were analysed retrospectively after approval of the local ethics committee, in accordance with the Declaration of Helsinki. Patients were diagnosed by an ocular oncologist based on fundus photography, ocular ultrasound and fluorescein angiography. The patients were selected to provide a clinically representative range in tumour size, shape and location. Patients were 62 ± 10 years old and 57 % were male. A wide range of tumour sizes was present, ranging from The American Joint Committee on Cancer (AJCC, 8th edition) stage T1 up to T4, with most patients in stages T2 (40 %) and T3 (40 %) [30]. 28 % of patients had an anteriorly located tumour and most tumours were dome-shaped (68 %), followed by mushroom-shaped (16 %) and flat (16 %). Patients were treated with either 106-Ruthenium brachytherapy (32 %) or PBT (68 %). The average time between ultrasound and MRI was 14 ± 11 days.

2.1. Image acquisition

3DT1gd and 3DT2-weighted images, both with acquisition voxel size of $0.8 \times 0.8 \times 0.8$ mm^3, were acquired to an earlier described protocol [15,16]. Ultrasound images were obtained by an ocular oncologist [25]. Details on image acquisition are further described in the Supplementary Materials.

2.2. Tumour delineation

Delineations were performed semi-automatically on the 3D T1gd and T2-weighted images using an in-house developed analysis pipeline in MeVisLab (MeVis Medical Solutions, Bremen, Germany) using a subdivision surface fit [26,31] (Fig. 1a-b). Areas which were hypointense compared to the vitreous on T2 and enhancing on T1gd compared to the native T1 were considered tumour.

The globe, defined as a combination of the vitreous, lens and tumour, was delineated in a similar fashion (Fig. 2a-b, yellow contour). Since clinical ultrasound measurements include the sclera, the outer sclera boundary at the tumour base was delineated as well (Fig. 2c). Based on the clinical evaluation of the MR-images by a neuro-radiologist with 20 years of experience (BV), an ophthalmic MRI expert with 9 years of experience (JWB) verified, and if necessary corrected, all contours.

2.3. Automatic 3D MRI measurements

In a pilot study, further described in the Supplementary Materials, we developed 3D definitions of tumour prominence and base. In short, three different 3D definitions of the tumour prominence and three different LBD definitions were evaluated in a multidisciplinary tumour board, consisting of ocular oncologists, radiation oncologists, clinical physicists and radiologists (BV, TV, MM, GL, CR, JWB). As these definitions were based on the 3D tumour contours, the resulting dimensions were not restricted to an individual slice of the MR-images. These definitions provided different approaches on how to define the tumour base and apex, e.g. point closest to the eye centre or point most distant from

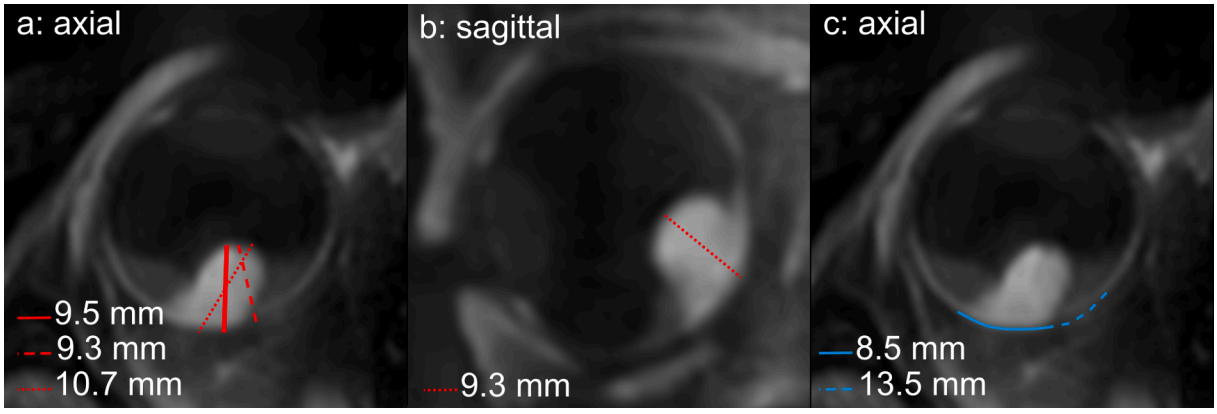

Fig. 1. Several measuring planes on T1gd-weighted MRI for a mushroom shaped UM. (a) Three possible prominence measurements in the axial plane for a complexly shaped tumour: starting with the point closest to the centre of the eye (solid, the definition used in this study), parallel with the main tumour axis (dotted) and including the overhanging part of the tumour (dashed). (b) An evaluation of the same tumour in the sagittal plane resulted in a different measurement. (c) For obliquely oriented tumours, several base definitions are possible depending on whether the overhanging part is included as tumour base.

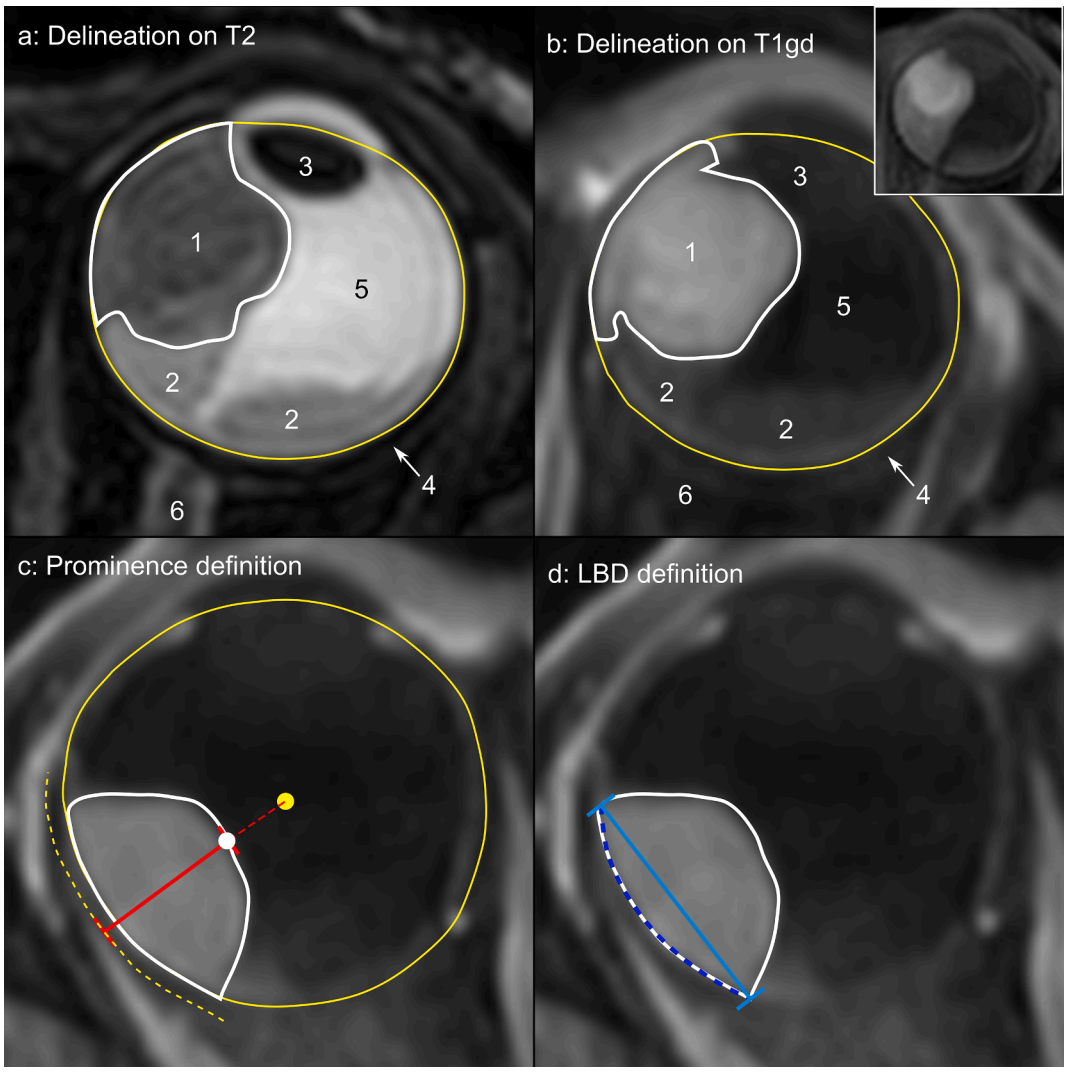

Fig. 2. Tumour (white contour) and globe (defined as combination of vitreous, lens and tumour, yellow contour) were delineated on T2-weighted (a) and contrast-enhanced T1-weighted (T1gd) (b) images, with the native T1-weighted image used as a reference (inset). Anatomical structures are marked as follows: (1) tumour, (2) retinal detachment, (3) lens, (4) sclera (hypointense layer), (5) vitreous, (6) optic nerve. Tumour prominence (c, red line) and largest basal diameter (d, blue line) were automatically determined. (c) Tumour prominence was measured from the tumour apex (white dot) to the sclera (dashed yellow line) (centre-based definition, Appendix A). (d) LBD was the largest Euclidean distance between two points in the tumour base (base: dashed line, measurement: solid line). In this image, the axial plane was shown as an example, whereas the tumour delineation was evaluated in the axial, sagittal and coronal plane. (For interpretation of the references to colour in this figure legend, the reader is referred to the web version of this article.)

the sclera. The evaluation of these definitions in 25 patients showed comparable measurements for patients with rotational-symmetric tumours. However, in the asymmetric tumours, some of the definitions resulted in measurement which did not conform the current clinical consensus. For example, defining the apex as the point most distant from the sclera resulted in an oblique prominence measurement which could not be used for radiotherapy planning purposes (Supplementary Fig. 1). The multidisciplinary evaluation of the definitions resulted in one prominence and one tumour base definition which provided visually acceptable measurements in all patients.

Based on the results of this pilot study, the tumour apex was defined as the point of the tumour contour closest to the centre of the globe (Fig. 2c). The prominence was measured along the line between the centre of the globe and the tumour apex (Fig. 1a, solid red line) and included the sclera to match the clinical convention at our centre.

LBD was defined as the largest Euclidean distance between two points in the tumour base (Fig. 2d, base: dashed line, LBD: solid line), which was defined as all points of the tumour contour less than 2 mm distant from the inner sclera contour, in order to create a robust tumour base. SBD was the largest distance between two points in the tumour base, perpendicular to the LBD.

For all patients the prominence, LBD and SBD were automatically determined using the T1gd- and T2-based 3D contours in Python (version 3.7.6) (Supplementary Materials).

2.4. Manual MRI measurements

In order to assess how these automatic 3D measurements relate to the currently used manual assessments, the prominence and LBD were measured manually on the T1gd-weighted images. For the prominence, the clinical measurement was used, measured perpendicular to the sclera [25]. For the LBD, the measurements were repeated on the delineated tumour contour, to avoid the confounding effect of a different tumour boundary interpretation [27]. For each patient, the angle between the lines of manual and the automatic measurement was determined.

2.5. Statistical analysis

Automatic T1gd prominence and LBD measurements were compared to manual MRI measurements. Additionally, automatic prominence and LBD were compared between T1gd and T2. Furthermore, the automatic T1gd and clinical ultrasound measurements were compared for prominence, LBD and SBD. For the prominence, differences > 0.5 mm and for the diameters, differences > 1.0 mm were considered clinically significant [25]. Medians and 25th–75th percentiles of the automatic-manual, T1gd-T2 and T1gd-ultrasound differences were assessed, as non-normality was demonstrated with a Shapiro-Wilk test (e.g. $p = 0.0003$ for the ultrasound-T1gd prominence comparison). Results for anterior tumours, defined as having a centre of mass in the anterior 50 % of the globe, were assessed separately. Additionally, tumours where the full extent could not be accurately determined on MRI or ultrasound, e.g. due to a flat tumour or a limited penetration depth or limited field of view (FOV) of the ultrasound transducer, were marked (Supplementary Fig. 2) [25].

3. Results

Representative examples of automatic prominence and LBD measurements on T2 and T1gd, and the corresponding ultrasound measurements, are shown in Fig. 3, with an overview of the primary outcomes. All comparisons and individual measurements for all patients can be found in the Supplementary Materials.

On T1gd, manual and automatic prominence measurements were comparable (median absolute difference 0.3 mm, Fig. 4a), with differences > 0.5 mm for 8/25 patients. The median absolute difference between automatic and manual LBD measurements was 0.5 mm, with differences > 1.0 mm for 14/25 patients (Fig. 4b). Larger differences were found in patients where the manual measurement was performed in a different plane than the automatic measurement (Fig. 4c). The mean angle between the manual and automatic measurement was 26 degrees (Fig. 4c, Supplementary Fig. 3).

Due to a limited penetration depth of the UBM transducer, the tumour apex was not visible in 2/25 patients, both of which had an anteriorly located tumour (Supplementary Fig. 2a). The full extent of the tumour base did not fit within the ultrasound's field of view for 9/25 patients, of which 7 had an anteriorly located tumour (Supplementary Fig. 2b). In 3/4 patients with an ultrasound prominence < 4 mm, the extent of the tumour base was difficult to assess on MRI.

The difference between ultrasound- and automatic T1gd-based prominence was > 0.5 mm in 6/25 patients, with a median absolute difference of 0.4 and 0.3 mm for anterior and posterior tumours, respectively (Fig. 5a). A retrospective re-evaluation of the ultrasound and fundus images of the patient with the largest difference (1.3 mm), showed that a haemorrhage at the tumour apex was erroneously

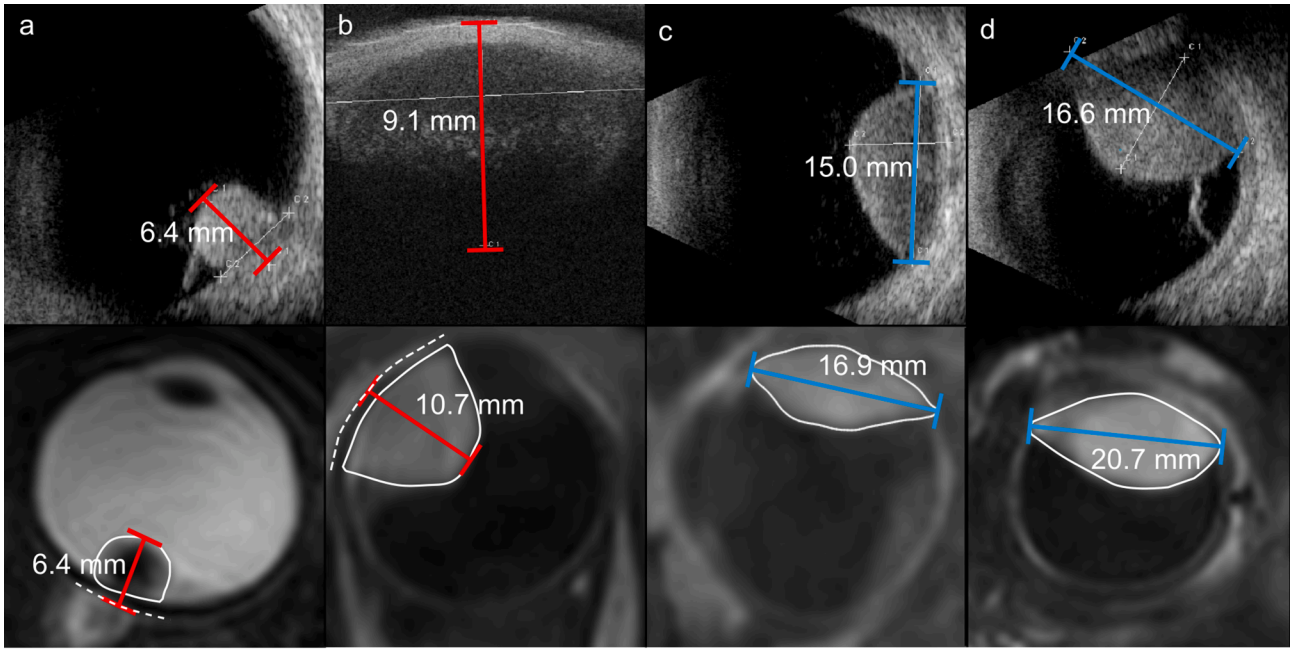

e

Median (max) absolute difference [mm]		T2 – T1gd	US – T1gd	US – T2	Manual – automatic (MRI T1gd)
Prominence	Entire group	0.3 (0.9)	0.3 (1.6)	0.4 (1.3)	0.3 (0.9)
	Anterior	0.3 (0.6)	0.4 (1.6)	0.6 (1.3)	0.2 (0.7)
	Posterior	0.3 (0.9)	0.3 (1.3)	0.4 (0.7)	0.3 (0.9)
LBD	Entire group	1.7 (6.7)	1.1 (7.6)	1.1 (6.8)	0.5 (5.3)
	Anterior	1.0 (4.1)	1.6 (4.5)	1.6 (4.4)	0.5 (1.4)
	Posterior	1.8 (6.7)	1.0 (7.6)	1.1 (6.8)	0.5 (5.3)

Fig. 3. Four typical examples of ultrasound (upper images) and MRI measurements (lower images) from four different patients and an overview of the main comparisons. (a) T2 and ultrasound measurements were similar. (b) T1gd prominence was larger for an anteriorly located tumour for which the extent was not entirely visible on UBM. (c) T1gd LBD was larger than on ultrasound for a tumour whose extent was visible on both modalities. (d) T1gd LBD was larger than on ultrasound and extent was not entirely visible on ultrasound. (e) Overview of the main comparisons performed in this study: automatic T2 – automatic T1gd, ultrasound (US) – automatic T1gd, ultrasound – automatic T2, manual T1gd – automatic T1gd.

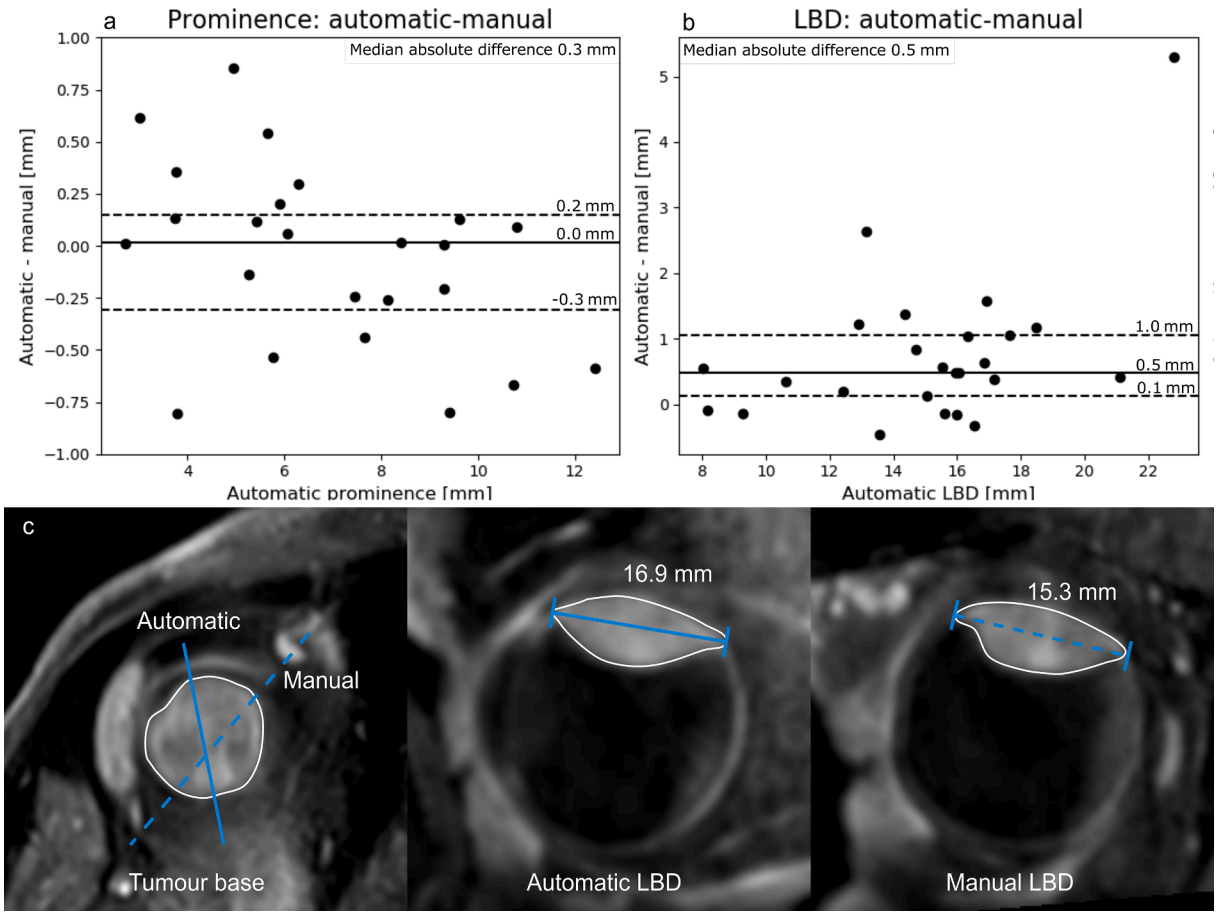

Fig. 4. (a) Differences between automatic and manual prominence measurements. (b) Differences between automatic and manual LBD measurements. (c) Manually determining the plane of the largest basal diameter proved to be difficult due to the curved tumour base. As a result, manual measurements generally underestimated the LBD.

included as tumour on ultrasound (Supplementary Fig. 4). For the remaining patients the largest absolute difference of 0.9 mm was found in a patient with an anteriorly located tumour, for which the apex was visible on ultrasound, with a prominence of 13.3 mm on ultrasound and 12.4 mm on MRI. Differences between T1gd- and T2-based prominence were small: for 6/25 patients, the difference was $>$ 0.5 mm, with a median absolute difference of 0.3 mm and a maximum of 0.9 mm (Fig. 5b).

Compared to ultrasound, 16/25 of LBD measurements were $>$ 1.0 mm larger on the automatic T1gd measurement (Fig. 3c). Median absolute differences between ultrasound and T1gd (Fig. 5c) were 0.9 mm for posteriorly located tumours and 1.6 mm for anteriorly located tumours. Slightly larger differences were found for the SBD, which resulted in a median absolute difference of 1.3 mm (maximum 4.6 mm, Supplementary Fig. 5).

Differences between automatic T2 and automatic T1gd LBD were $>$ 1.0 mm in 15/25 patients, with 13/15 being larger on T1gd. A median absolute difference of 1.6 mm was found between the two sequences (Fig. 5d). Often, peritumoral choroidal enhancement was visible on T1gd, which consequently was included as tumour, while this was not considered tumour on T2 and ultrasound (Fig. 6b-c). T2-based LBD measurements were more in agreement with ultrasound (median absolute difference 0.4 mm), compared to T1gd-based measurements (Supplementary Fig. 6). These smaller diameters on T2 were also reflected in the tumour volumes: tumour volume was larger on T1gd for 20/25 patients (average volume difference 18 %).

4. Discussion

With this study, we proposed an unambiguous 3D-imaging based prominence and base definition for treatment planning of uveal melanoma, which takes the requirements for brachytherapy and PBT planning into account [25,32,33], and which poses an extension of an earlier study [34], which assumed a dome shaped tumour with a circular base.

The proposed prominence and base definitions were considered appropriate by the multidisciplinary tumour board in our cohort of 25 patients. Although the cohort contained a variety of tumour sizes and shapes, we noted that in none of the obliquely oriented tumours, the LBD contained the overhanging part. As a result, the effects from overhanging parts were not reflected in the LBD assessments. Accurately incorporating overhanging parts in directions other than the LBD measurement axis, will however be beneficial for PBT, where similar discrepancies have been reported describing the tumour-marker relation [25]. We anticipate that the proposed definition may result in erroneous measurements for very prominent UM, with the centre of the eye within the mass. Nonetheless, the proposed prominence definition proved to be robust for variations in the location of the centre of the eye (Supplementary Fig. 7).

As the proposed automatic measurement methods are independent of field strength they are also applicable for patients scanned at lower field strengths than 3 T. In this study, subjects were scanned with closed eyes, as a previous comparison between different protocols showed that, while the use of a cued blinking protocol [35] results in less motion artefacts in some patients, not all patients are able to adhere to such a protocol, resulting in overall degraded image quality [36].

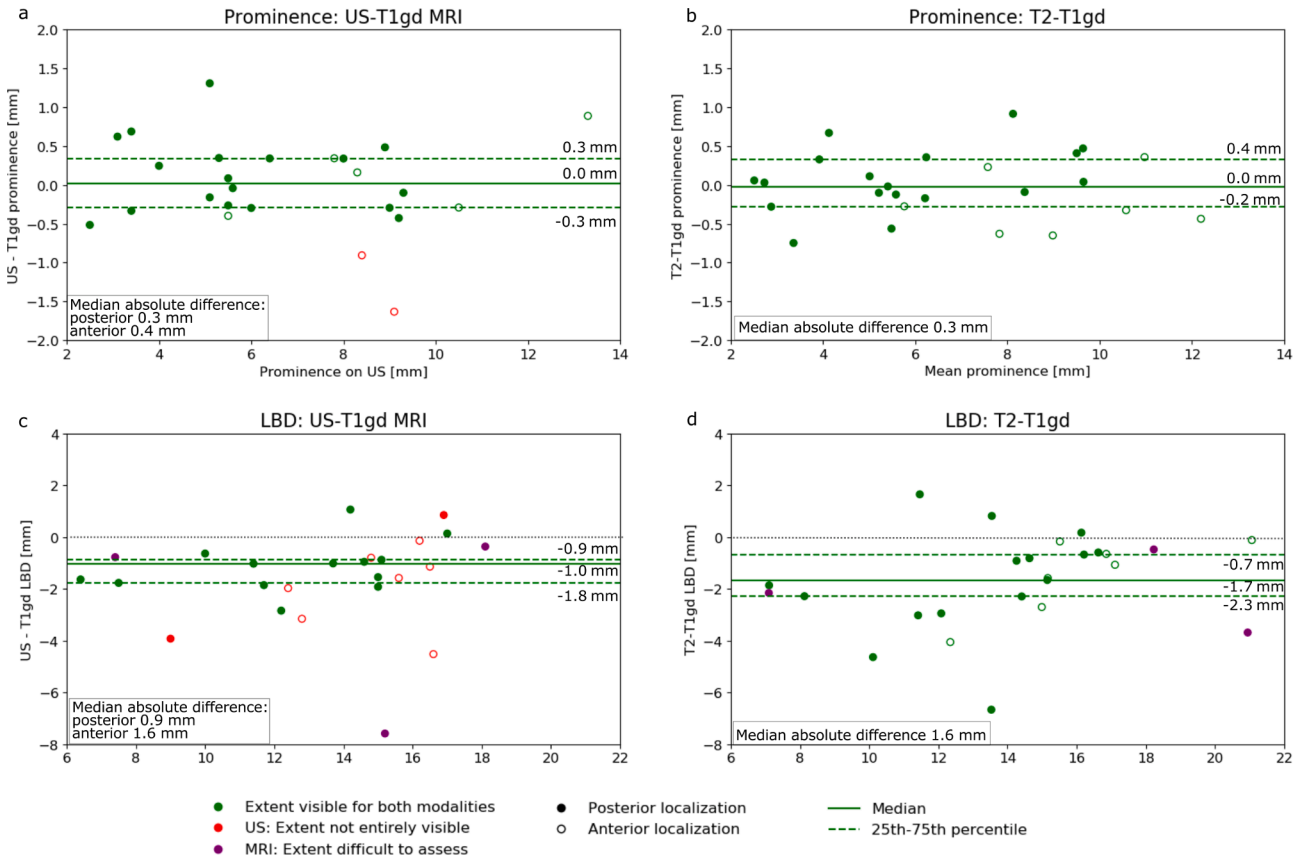

Fig. 5. Comparison of prominence and LBD between ultrasound and MRI. (a) For the prominence, ultrasound-T1gd differences were largest in anteriorly located tumours that were not fully visible on ultrasound. The largest prominence difference of 1.3 mm was caused by the erroneous inclusion of haemorrhage in the tumour prominence on ultrasound (Supplementary Figure 3). (b) Absolute differences between T1gd and T2 prominence measurements were < 0.5 mm in 19/25 patients. (c) Comparing ultrasound and T1gd MRI, LBD was larger on T1gd MRI in 22/25 patients. (d) Comparing LBD between T2 and T1gd, LBD was larger on T1gd in 22/25 patients.

As part of the data was acquired as part of regular clinical care, the MRI and ultrasound were not acquired on the same day for most patients. However, we expect the impact of this delay to be limited, as UM are known to be slow growing tumours [37,38], which is confirmed by the accordance in prominence measurements between both modalities.

In general, tumour prominence measurements agreed well across modalities if tumour extent was entirely visible, with all interquartile ranges within half the MRI acquisition voxel size. This corresponds to the recently reported interobserver delineation variation of 0.4 mm of ocular MRI [27] and is smaller than the reproducibility of B-mode ultrasound of 0.6 mm [13,14]. In our study, the largest prominence differences were found in patients for whom the tumour apex was not visible on ultrasound. This particularly occurred in patients with anteriorly located tumours imaged with a UBM probe, which has a limited penetration depth due to its higher frequency (50 MHz). For these patients, MRI was considered to be more accurate. Previous studies by Ferreira and Schueller [16,39] reported similar prominence measurements, although measurement methods differed.

Automatic LBD measurements were generally larger than manual MRI measurements, which were often performed in a plane not containing the largest diameter. Since the LBD can, by definition, not be overestimated, the automatic measurement was considered more accurate. However, since 68 % of the differences were < 1 mm, manual measurements are generally sufficient, especially given the known interobserver variability of the tumour-choroid interface on MRI of 0.6 mm [27]. On T1gd, peritumoral enhancement was included, which was invisible on T2, resulting in larger measurements on T1gd (median absolute difference 1.7 mm). Although the enhancement could be inflammatory of origin, it could also correspond to a small flat tumour extension. We therefore recommend to include these areas as tumour, until histopathology proves otherwise.

Generally, we found larger LBDs on T1gd than on ultrasound, with differences largest in anteriorly located tumours, especially when the full tumour extent was not visible on ultrasound. These differences can partly be explained by manual definition of the plane of the LBD of the ultrasound exam, which similar to the manual MRI measurements, might miss the actual largest diameter, with the added difficulty that no 3D visualisation can be made with ultrasound. In some patients the peritumoral choroidal enhancement observed on T1gd was included on ultrasound (Fig. 6c), while in other patients it was not (Fig. 6d). This inconsistency leads to uncertainties in the LBD measurement of flat UM as well, with differences between T1gd and ultrasound up to 7.6 mm. In 3/4 patients with flat UM, the MRI-report explicitly mentioned that the tumour extent was difficult to assess, confirming previous findings that MRI of flat melanoma can be difficult [16,25,34,40,41]. However, on ultrasound, the extent of these flat tumours is also not clearly visible. Therefore, optical validation of the flat tumour extent, which can be measured on some fundus and OCT imaging modalities [10], or increased margins, is necessary. For the SBD larger discrepancies with ultrasound were observed than for the LBD, however, the resulting ellipsoid model is more accurate than a circular model based on the LBD alone [8,9,42–45].

The clinical impact of the observed differences between ultrasound and MRI will depend on the application, and therefore an MRI-scan will not be needed for all patients. In general, we recommend to perform an MRI when the tumour extent is not fully visible on ultrasound, which was most often seen in anteriorly located tumours. For treatment selection, the effect of incorporating the MRI-based measurements

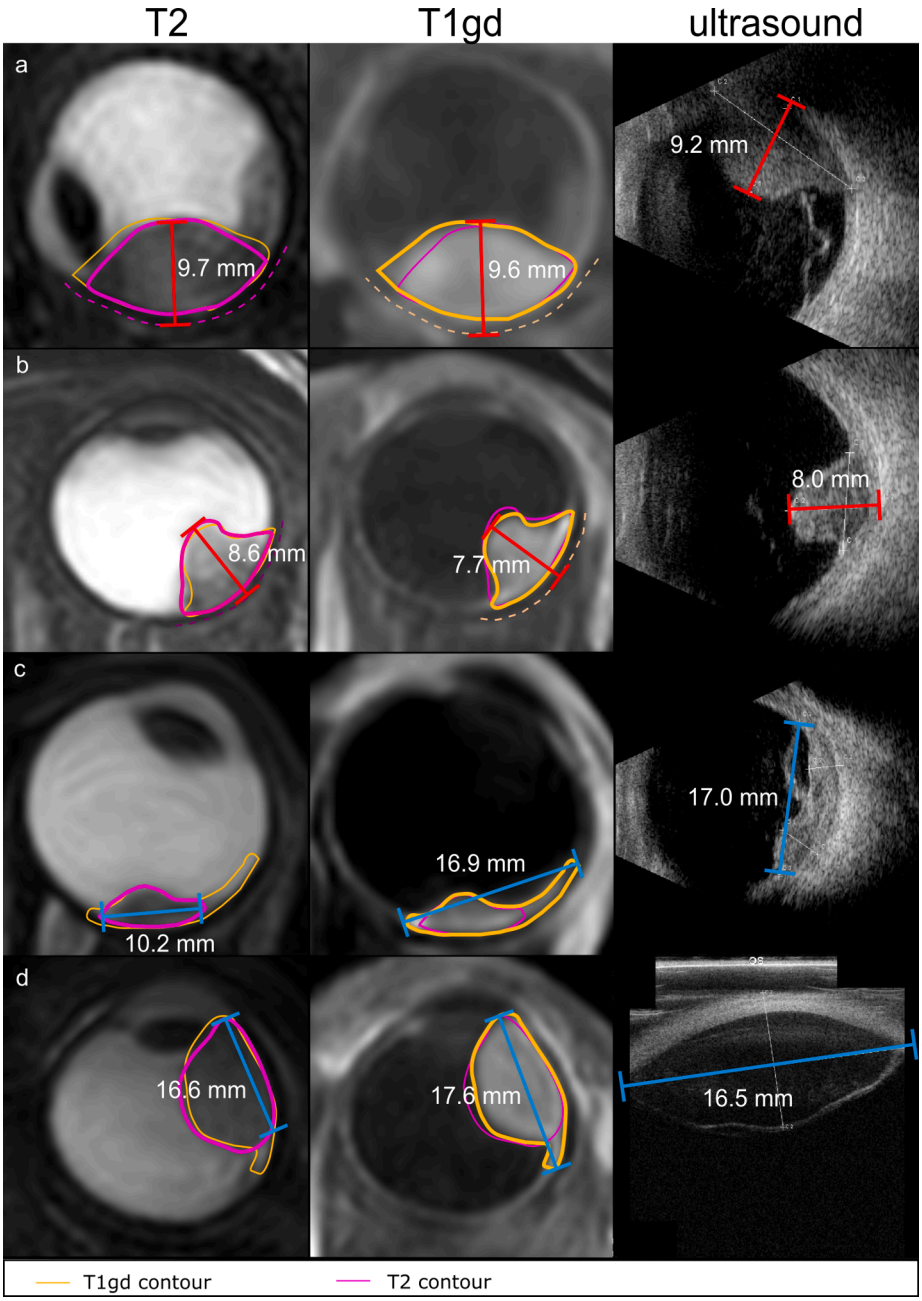

Fig. 6. Prominence and LBD measurement on T2-weighted MRI (left column), T1gd-weighted MRI (middle column) and US (right column). (a) Prominence was generally similar on T1gd and T2. (b) The largest difference between T2 and T1gd prominence was 0.9 mm. (c,d) LBD was generally larger on T1gd.

proposed in this study will depend on the type of treatments that are available. When a 0.5 mm change in prominence or 1 mm change in LBD can result in a shift of optimal treatment modality [19,46], we advise to perform an MRI with automatic T1gd measurements to confirm the ultrasound measurements. Although the benefit of including MRI in radiotherapy planning requires further study, we expect less benefit for patients treated with brachytherapy, due to the limited degrees of freedom with the currently available applicators. For PBT, however, the currently relatively large margins of up to 3 mm are in part needed for the uncertainties introduced by the ultrasound measurements [47–49]. Given the earlier reported benefits of including MRI for ocular PBT planning, we would recommend to perform an MRI for these patients and use the proposed 3D prominence and basal diameter definitions to resolve the discrepancies observed for complexly shaped tumours between MRI and ultrasound [25], especially until fully image-based 3D treatment planning systems for UM are clinically available [21,50–52].

In conclusion, 3D MRI-based tumour measurements were comparable to 2D ultrasound-based measurements. For anteriorly located tumours, MRI was more accurate. Furthermore, the methods proposed in this paper can contribute to a more personalized, image-based, radiotherapy planning for ocular oncology patients.

Funding

This study was supported by the LSBS, ANVVB and Oogfonds that contributed through UitZicht. These foundations provided unrestricted grants and had no role in the design or conduct of this research.

Declaration of Competing Interest

The authors declare the following financial interests/personal relationships which may be considered as potential competing interests: J. W.M. Beenakker received research support from Philips Healthcare. The other authors do not have any interests to declare.

Appendix A. Supplementary data

Supplementary data to this article can be found online at https://doi.org/10.1016/j.phro.2022.11.001.

References

[1] Jager MJ, Shields CL, Cebulla CM, Abdel-Rahman MH, Grossniklaus HE, Stern MH, et al. Uveal melanoma. Nat Rev Dis Primers 2020;6:24. https://doi.org/10.1038/s41572-020-0158-0.

[2] Yang J, Manson DK, Marr BP, Carvajal RD. Treatment of uveal melanoma: where are we now? Ther Adv Med Oncol 2018. https://doi.org/10.1177/1758834018757175.

[3] Kaliki S, Shields CL. Uveal melanoma: relatively rare but deadly cancer. Eye 2017;31:241–57. https://doi.org/10.1038/eye.2016.275.

[4] Mishra KK, Daftari IK. Proton therapy for the management of uveal melanoma and other ocular tumors. Chin Clin Oncol 2016;5:50. https://doi.org/10.21037/cco.2016.07.06.

[5] Mor JM, Semrau R, Baus W, Koch KR, Schaub F, Cursiefen C, et al. CyberKnife(R): new treatment option for uveal melanoma. Ophthalmologe 2018;115:302–8. https://doi.org/10.1007/s00347-017-0560-5.

[6] Parker T, Rigney G, Kallos J, Stefko ST, Kano H, Niranjan A, et al. Gamma knife radiosurgery for uveal melanomas and metastases: a systematic review and meta-analysis. Lancet Oncol 2020;21:1526–36. https://doi.org/10.1016/S1470-2045(20)30459-9.

[7] Hrbacek J, Mishra KK, Kacperek A, Dendale R, Nauraye C, Auger M, et al. Practice patterns analysis of ocular proton therapy centers: The International OPTIC Survey. Int J Radiat Oncol Biol Phys 2016;95:336–43. https://doi.org/10.1016/j.ijrobp.2016.01.040.

[8] Furdova A, Babal P, Kobzova D, Zahorjanova P, Kapitanova K, Sramka M, et al. Uveal melanoma survival rates after single dose stereotactic radiosurgery. Neoplasma 2018;65:965–71. https://doi.org/10.4149/neo_2018_171209N808.

[9] Gass JD. Comparison of uveal melanoma growth rates with mitotic index and mortality. Arch Ophthalmol 1985;103:924–31. https://doi.org/10.1001/archopht.1985.01050070050028.

[10] Solnik M, Paduszynska N, Czarnecka AM, Synoradzki KJ, Yousef YA, Choragiewicz T, et al. Imaging of uveal melanoma-current standard and methods in development. Cancers 2022;14. https://doi.org/10.3390/cancers14133147.

[11] Amin FES, Greene F. AJCC Cancer Staging Manual. Eighth edition. New York: Springer; 2017.

[12] Kaliki S, Shields CL, Shields JA. Uveal melanoma: estimating prognosis. Indian J Ophthalmol 2015;63:93–102. https://doi.org/10.4103/0301-4738.154367.

[13] Char DH, Kroll S, Stone RD, Harrie R, Kerman B. Ultrasonographic measurement of uveal melanoma thickness: interobserver variability. Br J Ophthalmol 1990;74:183–5. https://doi.org/10.1136/bjo.74.3.183.

[14] Haritoglou C, Neubauer AS, Herzum H, Freeman WR, Mueller AJ. Interobserver and intraobserver variability of measurements of uveal melanomas using standardised echography. Br J Ophthalmol 2002;86:1390–4. https://doi.org/10.1136/bjo.86.12.1390.

[15] Kamrava M, Sepahdari AR, Leu K, Wang PC, Roberts K, Demanes DJ, et al. Quantitative multiparametric MRI in uveal melanoma: increased tumor permeability may predict monosomy 3. Neuroradiology 2015;57:833–40. https://doi.org/10.1007/s00234-015-1546-0.

[16] Ferreira TA, Jaarsma-Coes MG, Marinkovic M, Verbist B, Verdijk RM, Jager MJ, et al. MR imaging characteristics of uveal melanoma with histopathological validation. Neuroradiology 2022;64:171–84. https://doi.org/10.1007/s00234-021-02825-5.

[17] Foti PV, Travali M, Farina R, Palmucci S, Spatola C, Raffaele L, et al. Diagnostic methods and therapeutic options of uveal melanoma with emphasis on MR imaging-Part I: MR imaging with pathologic correlation and technical considerations. Insights Imaging 2021;12:66. https://doi.org/10.1186/s13244-021-01000-x.

[18] Niendorf T, Beenakker JM, Langner S, Erb-Eigner K, Bach Cuadra M, Beller E, et al. Ophthalmic magnetic resonance imaging: where are we (heading to)? Curr Eye Res 2021;46:1251–70. https://doi.org/10.1080/02713683.2021.1874021.

[19] Beenakker JW, Ferreira TA, Soemarwoto KP, Genders SW, Teeuwisse WM, Webb AG, et al. Clinical evaluation of ultra-high-field MRI for three-dimensional visualisation of tumour size in uveal melanoma patients, with direct relevance to treatment planning. MAGMA 2016;29:571–7. https://doi.org/10.1007/s10334-016-0529-4.

[20] Ferreira TA, Grech Fonk L, Jaarsma-Coes MG, van Haren GGR, Marinkovic M, Beenakker JM. MRI of uveal melanoma. Cancers 2019;11. https://doi.org/10.3390/cancers11030377.

[21] Marnitz S, Cordini D, Bendl R, Lemke AJ, Heufelder J, Simiantonakis I, et al. Proton therapy of uveal melanomas: intercomparison of MRI-based and conventional treatment planning. Strahlenther Onkol 2006;182:395–9. https://doi.org/10.1007/s00066-006-1512-1.

[22] Cuesta Cuesta AB, Martin Rios MD, Noguero Meseguer MR, Garcia Velasco JA, de Matias MM, Bartolome Sotillos S, et al. Accuracy of tumor size measurements performed by magnetic resonance, ultrasound and mammography, and their correlation with pathological size in primary breast cancer. Cir Esp (Engl Ed) 2019;97:391–6. https://doi.org/10.1016/j.ciresp.2019.04.017.

[23] Taydas O, Durhan G, Akpinar MG, Demirkazik FB. Comparison of MRI and US in tumor size evaluation of breast cancer patients receiving neoadjuvant chemotherapy. Eur J Breast Health 2019;15:119–24. https://doi.org/10.5152/ejbh.2019.4547.

[24] Cha MJ, Lee MW, Cha DI, Kim JH, Rhim H, Cho YK, et al. Size discrepancy between sonographic and computed tomographic/magnetic resonance imaging measurement of hepatocellular carcinoma: the necessity of tumor size measurement standardization. J Ultrasound Med 2013;32:1703–9. https://doi.org/10.7863/ultra.32.10.1703.

[25] Jaarsma-Coes MG, Ferreira TA, Marinkovic M, Vu THK, van Vught L, van Haren GR, et al. Comparison of MRI-based and conventional measurements for proton beam therapy of uveal melanoma. Ophthalmol Retina 2022. https://doi.org/10.1016/j.oret.2022.06.019.

[26] Hassan MK, Fleury E, Shamonin D, Fonk LG, Marinkovic M, Jaarsma-Coes MG, et al. An automatic framework to create patient-specific eye models from 3D magnetic resonance images for treatment selection in patients with uveal melanoma. Adv Radiat Oncol 2021;6:100697. https://doi.org/10.1016/j.adro.2021.100697.

[27] Jaarsma-Coes M, Klaassen L, Verbist BM, Vu THK, Klaver YLB, et al. Inter-Observer variability in MR-based target volume delineation of uveal melanoma. submitted. 2022.

[28] Kumar S, Holloway L, Boxer M, Yap ML, Chlap P, Moses D, et al. Variability of gross tumour volume delineation: MRI and CT based tumour and lymph node delineation for lung radiotherapy. Radiother Oncol 2021;167:292–9. https://doi.org/10.1016/j.radonc.2021.11.036.

[29] Song Y, Erickson B, Chen X, Li G, Wu G, Paulson E, et al. Appropriate magnetic resonance imaging techniques for gross tumor volume delineation in external beam radiation therapy of locally advanced cervical cancer. Oncotarget 2018;9:10100–9. https://doi.org/10.18632/oncotarget.24071.

[30] Kivelä TS, Grossniklaus HE, et al. Uveal melanoma. In: AJCC cancer staging manual. 8th edition. New York (NY): Springer; 2016. p. 805:17.

[31] Kitslaar Pieter H, Staring M, Lelieveldt BPF, van der Geest RJ. Segmentation of branching vascular structures using adaptive subdivision surface fitting. Proceedings Volume 9413, Medical Imaging 2015: Image Processing; 94133Z 2015. https://doi.org/10.1117/12.2082222.

[32] Collaborative Ocular Melanoma Study G. Comparison of clinical, echographic, and histopathological measurements from eyes with medium-sized choroidal melanoma in the collaborative ocular melanoma study: COMS report no. 21. Arch Ophthalmol 2003;121:1163-71. https://doi.org/10.1001/archopht.121.8.1163.

[33] Varian Medical Systems. Planning Reference Guide for Eclipse Ocular Proton Planning. 2007; 1–286.

[34] Via R, Hennings F, Pica A, Fattori G, Beer J, Peroni M, et al. Potential and pitfalls of 1.5T MRI imaging for target volume definition in ocular proton therapy. Radiother Oncol 2021;154:53–9. https://doi.org/10.1016/j.radonc.2020.08.023.

[35] Beenakker JWM, van Rijn GA, Luyten GPM, Webb AG. High-resolution MRI of uveal melanoma using a microcoil phased array at 7 T. NMR Biomed 2013;26:1864–9. https://doi.org/10.1002/nbm.3041.

[36] Tang MCY, Jaarsma-Coes MG, Ferreira TA, Zwirs-Grech Fonk L, Marinkovic M, Luyten GPM, et al. A comparison of 3 T and 7 T MRI for the clinical evaluation of uveal melanoma. J Magn Reson Imaging 2022;55:1504–15. https://doi.org/10.1002/jmri.27939.

[37] Augsburger JJ, Gonder JR, Amsel J, Shields JA, Donoso LA. Growth rates and doubling times of posterior uveal melanomas. Ophthalmology 1984;91:1709–15. https://doi.org/10.1016/s0161-6420(84)34088-x.

[38] Char DH, Kroll S, Phillips TL. Uveal melanoma. Growth rate and prognosis. Arch Ophthalmol 1997;115:1014–8. https://doi.org/10.1001/archopht.1997.01100160184007.

[39] Schueller P, Dogan A, Panke JE, Micke O, Willich N. Does the imaging method have an influence on the measured tumor height in ruthenium plaque therapy of uveal melanoma? Strahlenther Onkol 2005;181:320–5. https://doi.org/10.1007/s00066-005-1342-6.

[40] Beenakker JM, Rasch CRN. Letter to the Editor of Radiotherapy and Oncology regarding the paper titled "MRI and FUNDUS image fusion for improved ocular biometry in Ocular Proton Therapy" by Via et al. Radiother Oncol 2022. https://doi.org/10.1016/j.radonc.2022.08.018.

[41] Via R, Pica A, Antonioli L, Paganelli C, Fattori G, Spaccapaniccia C, et al. MRI and FUNDUS image fusion for improved ocular biometry in Ocular Proton Therapy. Radiother Oncol 2022;174:16–22. https://doi.org/10.1016/j.radonc.2022.06.021.

[42] Heilemann G, Fetty L, Dulovits M, Blaickner M, Nesvacil N, Georg D, et al. Treatment plan optimization and robustness of (106)Ru eye plaque brachytherapy using a novel software tool. Radiother Oncol 2017;123:119–24. https://doi.org/10.1016/j.radonc.2017.01.010.

[43] Studenski MT, Patel NV, Markoe A, Harbour JW, Samuels SE. Influence of tumor shape and location in eye plaque brachytherapy dosimetry. Brachytherapy 2020;19:249–54. https://doi.org/10.1016/j.brachy.2020.01.001.

[44] Tien CJ, Astrahan MA, Kim JM, Materin M, Chen Z, Nath R, et al. Incorporating patient-specific CT-based ophthalmic anatomy in modeling iodine-125 eye plaque brachytherapy dose distributions. Brachytherapy 2017;16:1057–64. https://doi.org/10.1016/j.brachy.2017.06.014.

[45] Daftari I, Aghaian E, O'Brien JM, Dillon W, Phillips TL. 3D MRI-based tumor delineation of ocular melanoma and its comparison with conventional techniques. Med Phys 2005;32:3355–62. https://doi.org/10.1118/1.2068927.
[46] Grech Fonk L, Ferreira TA, Webb AG, Luyten GPM, Beenakker JM. The economic value of MR-imaging for uveal melanoma. Clin Ophthalmol 2020;14:1135–43. https://doi.org/10.2147/OPTH.S238405.
[47] Damato B, Kacperek A, Errington D, Heimann H. Proton beam radiotherapy of uveal melanoma. Saudi J Ophthalmol 2013;27:151–7. https://doi.org/10.1016/j.sjopt.2013.06.014.
[48] Jung SK, Park YH, Shin DH, Kim HS, Jung JH, Kim TH, et al. Visual outcomes of proton beam therapy for choroidal melanoma at a single institute in the Republic of Korea. PLoS One 2020;15:e0242966.
[49] Marinkovic M, Pors LJ, van den Berg V, Peters FP, Schalenbourg A, Zografos L, et al. Clinical outcomes after international referral of uveal melanoma patients for proton therapy. Cancers 2021:13. https://doi.org/10.3390/cancers13246241.
[50] Fleury E, Trnkova P, Erdal E, Hassan M, Stoel B, Jaarma-Coes M, et al. Three-dimensional MRI-based treatment planning approach for non-invasive ocular proton therapy. Med Phys 2021;48:1315–26. https://doi.org/10.1002/mp.14665.
[51] Pfeiffer K, Dobler B, Rethfeldt C, Schlegel W, Bendl R. OCTOPUS: a planning tool for proton therapy of eye tumours. Phys Med 2001;17:59–62.
[52] Wulff J, Koska B, Janson M, Baumer C, Denker A, Geismar D, et al. Technical note: Impact of beam properties for uveal melanoma proton therapy-An in silico planning study. Med Phys 2022;49:3481–8. https://doi.org/10.1002/mp.15573.